Nanoscale Advances

ROYAL SOCIETY OF CHEMISTRY

PAPER

View Article Online
View Journal | View Issue

Cite this: *Nanoscale Adv.*, 2026, **8**, 2713

Insights into the adsorption performance of temozolomide on T-based 2D nanosheets from DFT and COSMO calculations

Md. Saydur Rahman Dostagir,[a] Afiya Akter Piya, *[a] Mehedi Hasan Opi,[a] Md. Ashik-E-Elahe[b] and Siraj Ud Daula Shamim [a]

Received 18th December 2025
Accepted 15th March 2026

DOI: 10.1039/d5na01147g

rsc.li/nanoscale-advances

In this study, density functional theory (DFT) was employed to investigate the adsorption behavior and electronic interaction characteristics of the anticancer drug temozolomide (TMZ) towards T-graphene (T-G), T-boron nitride (T-BN), T-aluminum nitride (T-AlN), and T-gallium nitride (T-GaN). The primary objective of this study was to determine the most efficient nanocarriers for TMZ delivery. Several parameters were calculated, such as the adsorption energy, desorption time, dipole moment, electronic properties and quantum molecular descriptors, under both gas phase and aqueous conditions. The results demonstrated that the S_1 configuration, in which TMZ is parallel to the nanosheets, provided the most favorable and stable interaction between TMZ and the nanosheets. Among the materials studied, the adsorption energy of T-AlN was strongest, at −1.56 eV. T-GaN also displayed favorable adsorption performance, with an adsorption energy of −1.16 eV. The HOMO–LUMO band gap reduced by 70.48% for T-AlN and 48.70% for T-GaN. These changes imply improved electronic conductivity and chemical reactivity. These properties are crucial for drug delivery. Furthermore, COSMO surface analysis revealed increased polarity and enhanced solubility of the drug-carrier complexes in aqueous media. This study suggests that T-AlN and T-GaN nanosheets could be suitable carriers for the anticancer drug TMZ.

1. Introduction

Cancer is a genetic disease that is increasingly common all over the world nowadays. It occurs when the body cells grow abruptly and spread to other body parts.[1] It is a genetic mutation that results in the disruption of normal cell function. Cancer can vary depending on the tissue or organ from which it arises. Many methods for treating cancers are available in medical science, such as surgery, chemotherapy, radiation therapy, immunotherapy, targeted therapy, and hormone therapy, and these are often used in combination.[2] The goal of cancer treatment is to either cure or shrink the tumor or stop it from spreading.[3] Chemotherapy and anticancer medications are specifically formulated to heal cancer patients by restraining the cancer cell development, and proliferation.[4] Nanotechnology is revolutionizing the field of cancer treatment, outperforming conventional chemotherapy.[5,6] Conventional drug delivery systems present issues such as poor drug solubility and bioavailability, rapid clearance or degradation in the body, and non-specificity for targeting, leading to side effects.[7] These drawbacks can be avoided by the use of nanomaterials by enhancing hydrophobic drug solubility, enabling sustained and controlled release, and facilitating targeted delivery to target tissues or cells.[8,9] Ideal nanocarriers should exhibit biocompatibility and low toxicity. They must possess a high theoretical drug-loading capacity and allow surface modification for targeted delivery. Additionally, they should provide controlled drug release, maintain stability under both storage and physiological conditions, and be either biodegradable or safely eliminated from the body without inducing toxicity.[10] Temozolomide (TMZ) is an oral alkylating chemotherapeutic agent used for the treatment of malignant brain tumors. Due to the small molecular size of the drug, it can easily cross the blood–brain barrier. Hence, it is one of the most effective drugs for central nervous system cancers. However, TMZ suffers from poor stability, uncontrolled release, and limited retention at the target site; it can also induce some common side effects, including nausea, vomiting, fatigue, and headache.[11]

Recently, 2D T-graphene (T-G), T-boron nitride (T-BN), T-aluminum nitride (T-AlN), and T-gallium nitride (T-GaN) materials have shown potential in the fields of drug adsorption and delivery.[12] The electronic flexibility and surface area make T-G an attractive candidate for non-covalent drug loading.[13,14] T-BN shares structural similarity with graphene but differs in that it has polar covalent bonds between boron and nitrogen atoms. It is expected that this polarity will enhance electrostatic interaction with polar functional groups, thereby

[a]*Department of Physics, Mawlana Bhashani Science and Technology University, Tangail-1902, Bangladesh. E-mail: afiya@mbstu.ac.bd*

[b]*Department of Computer Science and Engineering, Daffodil International University, Dhaka-1216, Bangladesh*

improving coupling with the nanocarrier and ensuring a uniform dispersion in solution.[15] In the past decade, the AlN nanostructure has received significant attention. It has some promising uses for field emitters, chemical sensors, and hydrogen storage.[16–18] AlN nanotubes have been widely researched as chemical sensors using DFT.[19,20] T-AlN and T-GaN both have mechanical robustness, tunable band gaps, and good thermal conductivity, enabling stable drug–carrier interactions and potential responsiveness to external stimuli.[21] Moreover, these materials are composed of abundant and relatively low-cost elements and can be synthesized using scalable fabrication routes, suggesting practical feasibility for biomedical applications.[22] Drug–nanomaterial interactions have been studied through computational methods.

Recent studies have investigated various nanosheet materials for anticancer drug delivery. Siqi *et al.* reported that T-BN and T-G nanosheets are promising drug carriers.[23] DFT calculations by Jouonang Létché *et al.* revealed that Al-doped boron nitride nanocages strongly interact with thalidomide, leading to enhanced adsorption stability and electronic sensitivity, thereby supporting the use of BN-based nanomaterials in drug delivery and sensing applications.[24] Wandji *et al.* demonstrated that BN- and AlN-based nanocages exhibit strong affinity toward temozolomide, with favorable adsorption energies and significant electronic response.[25] Ibrahim *et al.* suggest that $B_{12}N_{12}$ boron nitride nanocages effectively adsorb temozolomide, exhibiting strong interactions and potential for drug delivery.[26] Ibrahim *et al.* highlighted the potential of pristine graphene nanosheets for biomedical applications.[27] Based on dipole moment, work function, and COSMO analyses, Sakib *et al.* identified T-AlN and T-GaN nanosheets as suitable carriers.[28] Ortiz *et al.* found that carbon-doped gallium nitride (GaN-C) nanosheets perform better than AlN-C and BN-C for TMZ delivery.[29] Tamafo Fouegue *et al.* (2023) suggest that BC_{23} is a superior adsorbent of TMZ compared with some other nanomaterials, based on DFT studies.[30] Di Ma *et al.* (2024) showed that thiol-protected $Au_{12}(SCH_3)_9^+$ clusters strongly interact with TMZ and went on to highlight their potential for drug delivery.[31]

In this study, we used DFT to investigate the interactions between TMZ and some 2D nanosheets: T-G, T-BN, T-AlN, and T-GaN. The novelty of this work lies in exploring these emerging tetragonal 2D materials as potential drug-delivery carriers for TMZ, which have not been previously examined for this application. To assess the suitability of these nanosheets as drug-delivery carriers, the adsorption energy, electronic properties, charge-transfer characteristics, drug-release time and energy-gap variations are analyzed. For more details, we calculated the highest occupied molecular orbital (HOMO), lowest unoccupied molecular orbital (LUMO), Fermi level, work function, and density of states (DOS). The influence of the solvent environment is evaluated using the conductor-like screening model (COSMO) to simulate physiological conditions.

2. Computational details

All the calculations of the current study were performed using the DFT method in the DMol^3 module of Material Studio to investigate the adsorption characteristics and electronic properties of the anticancer drug TMZ on four different nanosheets, T-G, T-BN, T-AlN, and T-GaN, in both air and water media.[32] The Perdew–Burke–Ernzerhof (PBE) exchange–correlation function with the generalized gradient approximation (GGA) was used for the geometry optimizations and electronic structure computations.[33,34] To accurately describe the weak van der Waals interactions involved in physisorption processes, the Tkatchenko–Scheffler (TS) method was applied. The double numerical basis set with polarization (DNP) was chosen for all atoms due to its high accuracy and its effectiveness in minimizing the basis set superposition error (BSSE), making it comparable with the 6-31G** Gaussian basis set. The DFT semi-core pseudopotential (DSPP) was used to treat core electrons.[35] To ensure accurate and computationally efficient modeling of the nanosheets, a global cut-off radius of 5.0 Å was used for all calculations. Structural optimizations were performed using convergence thresholds of 1×10^{-5} Ha for the total energy, 0.002 Ha Å^{-1} for the maximum atomic force, and 0.005 Å for the maximum atomic displacement. Calculations were performed in both gas and aqueous phases, with the solvent effect in the latter modeled using a dielectric constant of 78.54 to represent water.[36,37]

The adsorption energy (E_{ad}) of TMZ on the nanosheets was calculated using the following equation:

$$E_{ad} = E_{complex} - E_{temozolomide} - E_{nanosheet}, \quad (1)$$

where $E_{complex}$ is the total energy of the drug-nanosheet complex, $E_{temozolomide}$ is the energy of the isolated TMZ molecule, and $E_{nanosheet}$ is the energy of the pristine nanosheet. Negative values of E_{ad} indicate favorable and spontaneous adsorption.

The electronic properties were evaluated by calculating the energy gap (E_g) between the highest occupied molecular orbital (HOMO) and the lowest unoccupied molecular orbital (LUMO):

$$E_g = E_{LUMO} - E_{HOMO}. \quad (2)$$

The change in the energy gap (ΔE_g) upon adsorption was used to assess the sensing behavior of the nanosheets, computed as follows:[38]

$$\Delta E_g = [(E_{nanosheet} - E_{complex})/E_{nanosheet}] \times 100. \quad (3)$$

To further analyze the chemical reactivity, the global quantum descriptors were determined, as follows:[39–43]

$$\text{The chemical potential, } \mu = -(E_{HOMO} + E_{LUMO})/2, \quad (4)$$

$$\text{Global hardness, } \eta = (E_{LUMO} - E_{HOMO})/2, \quad (5)$$

$$\text{Global softness, } S = \tfrac{1}{2}\eta, \quad (6)$$

$$\text{Electrophilicity index, } \omega = \mu^2/2\eta, \quad (7)$$

$$\text{Nucleophilicity index, } \nu = 1/\omega. \quad (8)$$

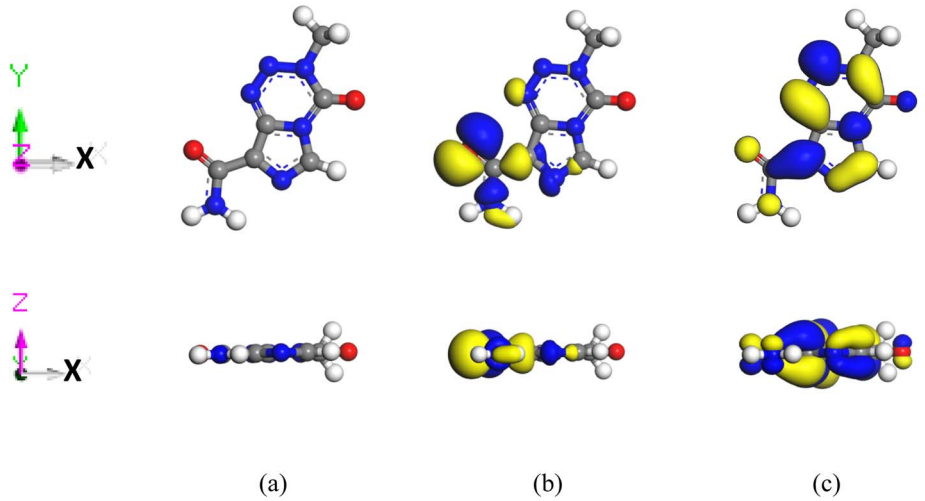

Fig. 1 Top and side views of the (a) optimized structure, (b) HOMO, and (c) LUMO of the TMZ drug molecule.

The charge transfer between TMZ and the nanosheets was investigated using Mulliken charge analysis to determine whether the drug acted as an electron donor or acceptor.

3. Results and discussion

3.1 Adsorption of TMZ on T-G nanosheet

In this study, geometric optimization of tetragonal nanosheets, including T-G, T-BN, T-AlN, and T-GaN, was performed in both gas and aqueous phases to simulate the physiological conditions for TMZ adsorption modeling. The bond angles and bond lengths of these nanosheets were evaluated by Sakib *et al.*[28]

TMZ (Fig. 1) is a clinically established chemotherapeutic agent for glioblastoma multiforme. It was selected due to its well-documented efficacy against malignant gliomas. Incorporating TMZ into nanosheet-based carriers aims to achieve sustained and controlled release, enhance drug stability, and improve targeted delivery to tumor tissues. Furthermore, the high surface-area-to-volume ratio and substantial drug-loading capacity of nanosheet structures facilitate efficient TMZ encapsulation and promote effective interactions with biological interfaces.

This research examined the incorporation of TMZ as an anticancer drug to assess the use of nanosheet-based systems for advanced treatment of brain tumors. To investigate the relation between TMZ and T-G, the adsorption energies (E_{ad}), adsorption distances (d), and charge-transfer (Q) characteristics were measured; the results are shown in Table 1. There are many possible positions for the TMZ to adsorb on the T-G surface. According to previous findings, drug molecules tend to adsorb more effectively onto nanosheets when arranged in a parallel configuration.[44] We took three possible positions for the TMZ on the T-G surface. The TMZ drug was placed parallel to the T-G (defined as S_1); perpendicular to the T-G, where the 2H atom of TMZ is toward the T-G (defined as S_2); and where the 3H atom of TMZ is perpendicular to the T-G (defined as the S_3 configuration). Fig. 2 shows the optimized structures of all the

Table 1 Calculated minimum interaction distance (d, in Å), adsorption energy (E_{ad}, in eV), and charge transfer (ΔQ, in e) between TMZ and nanosheets in the gas phase

		Gas phase			Water phase		
Nanosheets	States	d (Å)	E_{ad} (eV)	ΔQ (e)	d (Å)	E_{ad} (eV)	ΔQ (e)
T-G	S_1	2.79	−1.131	0.02	2.813	−0.91	0.01
	S_2	2.36	−0.225	0.001	—	—	—
	S_3	2.83	−0.298	0.01	—	—	—
T-BN	S_1	2.96	−1.044	−0.03	2.975	−0.86	−0.03
	S_2	2.29	−0.256	−0.01	—	—	—
	S_3	2.85	−0.259	0	—	—	—
T-AlN	S_1	1.99	−1.561	−0.02	1.97	−1.28	0.06
	S_2	2.13	−0.364	−0.04	—	—	—
	S_3	2.89	−0.247	−0.02	—	—	—
T-GaN	S_1	2.64	−1.161	0.04	2.671	−0.90	0.05
	S_2	2.93	−0.177	−0.02	—	—	—
	S_3	2.93	−0.252	−0.01	—	—	—

studied complexes. Positive adsorption energy indicates an endothermic process, whereas negative adsorption energy indicates an exothermic reaction. The adsorption energies were calculated using the eqn (1), indicating attractive and exothermic interactions with TMZ. The values obtained were −1.13 eV, −0.225 eV, and −0.298 eV for S_1, S_2 and S_3 configurations, respectively. When the value of E_{ad} is less than 1 eV, it indicates physical adsorption, whereas when it is larger than 1 eV, it shows chemical adsorption.[45] Accordingly, the S_1 configuration corresponds to chemisorption, while the S_2 and S_3 configurations are governed by physisorption. The stronger binding in the S_1 configuration implies enhanced structural stability of the drug-nanosheet complex, which is advantageous for efficient drug loading and stable immobilization of TMZ during the delivery process. The TMZ molecule prefers to adsorb on the T-G at distances of around 2.79 Å for S_1, 2.36 Å for S_2 and 2.83 Å for S_3 complexes. Electrons were transferred throughout TMZ and T-G during the interaction. The net charge

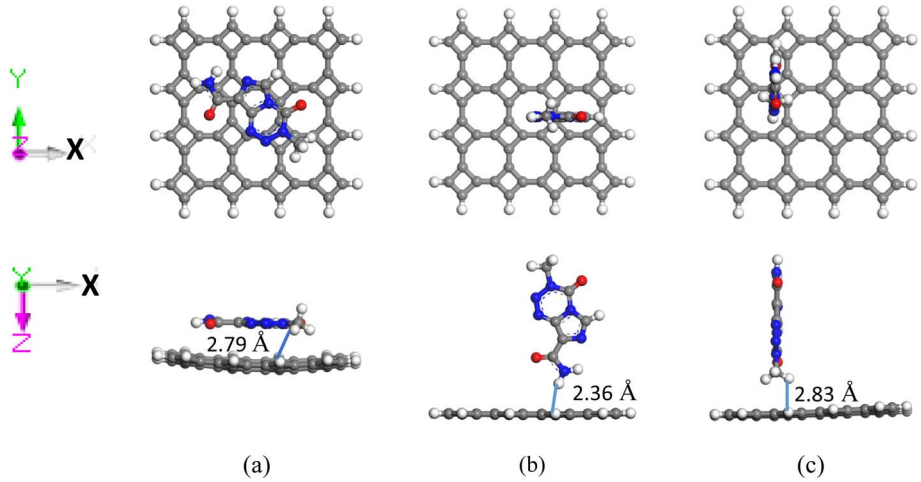

Fig. 2 Optimized geometries from the top and side views for the (a) S_1, (b) S_2, and (c) S_3 configurations of the TMZ/T-G complexes.

transfer (ΔQ) was calculated by using Mulliken charge analysis and the following equation, as reported in Table 1.

$$\Delta Q = Q_a - Q_b \quad (9)$$

where the terms Q_a and Q_b correspond to the charge on the drug molecule before and after its adsorption onto the nanosheet surface, respectively, and ΔQ quantifies the resulting charge difference. The drug molecule initially possesses zero net charge prior to adsorption, but it undergoes charge transfer, either gaining or losing electrons, after interaction with the nanosheets. The positive and negative values of net charges on the drug indicate the losses and gains of charge from the nanosheets, respectively. According to the Mulliken charge analysis, during the interaction of TMZ in these three configurations on the T-G nanosheets, a small amount of charge of about 0.02, 0.001, and 0.01e was transferred from TMZ to the proposed nanosheets, respectively. So, the TMZ drug molecule acts as an electron donor, and T-G acts as an electron acceptor. Therefore, the high negative values of the adsorption energies with low interaction distance and appreciable amount of charge transfer imply that the S_1 configuration of TMZ with the nanosheet exhibits the strongest and most favorable interaction, making it the most sensitive and promising configuration for drug adsorption.

Frontier molecular orbital (FMO) and energy gap (E_g) analyses were performed, and the results are tabulated in Table 2. Fig. 7 shows the FMO maps of the stable complexes of the TMZ/T-G. The HOMO and LUMO levels were located at −4.2 eV and −3.96 eV for T-G nanosheets, respectively. After adsorption of TMZ on the nanosheets, the HOMO and LUMO levels varied. For example, for the S_1 configuration, the HOMO levels were −4.23 eV, while the LUMO levels increased from −3.96 to −3.99 eV. The HOMO and LUMO gap, *i.e.*, the energy gap, was also calculated. It was found that the energy gap had remained

Table 2 HOMO energy (E_{HOMO}), LUMO energy (E_{LUMO}), and energy gap (E_g) in eV, change in energy gap (% ΔE_g), dipole moment (D.M.) in Debye (D), Fermi level energies (E_F) and work function (φ) in eV, and change in work function (% φ) for the studied complexes in the gas phase

Complexes	States	E_{HUMO} (eV)	E_{LUMO} (eV)	E_g (eV)	% ΔE_g	D.M. (D)	E_F (eV)	φ (eV)	% φ
TMZ		−5.92	−3.51	2.41	—	3.41	−4.71	4.71	—
T-G		−4.2	−3.96	0.24	—	0	−4.08	4.075	—
TMZ/T-G	S_1	−4.23	−3.99	0.24	1.24	2.43	−4.12	4.11	0.83
	S_2	−4.21	−3.96	0.25	3.32	1.71	−4.09	4.08	0.24
	S_3	−4.30	−4.06	0.24	0.83	3.63	−4.18	4.18	2.58
T-BN		−5.60	−1.72	3.88	—	0	−3.65	3.65	—
TMZ/T-BN	S_1	−5.58	−3.26	2.33	−39.98	2.77	−4.35	4.36	19.43
	S_2	−5.57	−3.31	2.26	−41.81	2.62	−4.36	4.36	19.57
	S_3	−5.69	−3.30	2.4	−38.33	3.33	−4.41	4.41	21.06
T-AlN		−5.1	−1.88	3.22	—	0	−3.39	3.39	—
TMZ/T-AlN	S_1	−4.88	−3.93	0.95	−70.48	3.7	−4.35	4.35	28.36
	S_2	−5.05	−3.43	1.63	−49.47	2.47	−4.16	4.16	22.67
	S_3	−5.15	−3.49	1.66	−48.38	3.3	−4.22	4.22	24.42
T-GaN		−5.04	−2.27	2.77	—	0	−3.55	3.55	—
TMZ/T-GaN	S_1	−4.94	−3.52	1.42	−48.70	2.76	−4.16	4.16	16.96
	S_2	−5.02	−3.35	1.67	−39.52	2.41	−4.09	4.09	15.14
	S_3	−5.08	−3.35	1.74	−37.24	3.52	−4.11	4.11	15.72

the same for S_1 configurations. The electronic properties, such as the HOMO and LUMO energies and the energy gaps, were also calculated in water media. The HOMO level is located at −4.59 eV for the T-G structure, but the LUMO level has a value of −4.34 eV before adsorption. After adsorption of the drug on the T-G nanosheet, the HOMO and LUMO levels were located at 4.58 and −4.33 eV, respectively. Compared to the gas phase, the adsorption behavior of TMZ on the T-G nanosheet is slightly enhanced in water phase. Low E_g molecules are more polarized and exhibit strong chemical reactivity and low kinetic stability.[46] As the energy gap for the T-G nanosheet increased after adsorption, the nanosheet shows a lower chemical reactivity towards the TMZ drug. Density of states (DOS) analysis provides a better understanding of the distribution of electronic states in a carrier complex as a function of energy. The DOS plots show that the energy gap increased after TMZ adsorption on the T-G nanosheet (Fig. 4). E_g is proportional to the number of conduction electrons (N), which can be converted into an electrical signal for drug detection. The equation can be written as follows:[47]

$$N = AT^{3/2} \times \exp(-E_g/2KT) \quad (10)$$

where K denotes the Boltzmann constant, and A (electrons/m^3/$k^{3/2}$) is also a constant.[48] From the equation, a lower E_g value is responsible for higher electrical conductivity, which can be converted into an electrical signal.

3.2 Adsorption of TMZ on T-BN nanosheets

This study assessed the suitability of the T-BN nanosheet as a potential nanocarrier for TMZ by modeling their interactions in the gas phase (Fig. 3). The calculated adsorption energies of TMZ on the T-BN surface are −1.044 eV, −0.256 eV, and −0.259 eV for the S_1, S_2, and S_3 configurations, respectively. Among the three configurations, the S_1 configuration exhibits the strongest interaction, indicating relatively strong binding between TMZ and the T-BN nanosheet. Similar values of adsorption energy were found by Di Ma *et al.*[31] Such interaction strength is beneficial for efficient drug loading and stable immobilization of TMZ during transport. In contrast, the weaker adsorption observed for the S_2 and S_3 configurations corresponds to physisorption. TMZ is adsorbed to the T-BN surface for the S_1 configuration at an equilibrium distance of 2.69 Å, which is close enough to permit strong interactions. It was determined *via* Mulliken charge analysis that charge transfer occurs from the TMZ drug towards the T-BN substrate, resulting in an approximate −0.028e, −0.028e, and −0.028e net electron donation, which reflects weak but non-negligible charge redistribution during adsorption. This charge transfer alters the electronic characteristics of the nanosheet, particularly in the vicinity of the Fermi level.

The pristine T-BN nanosheet has HOMO and LUMO levels at −5.602 eV and −1.723 eV, respectively, giving it a band gap (E_g) of 3.879 eV. Post-adsorption of TMZ led to −5.585 eV for HOMO and −3.257 eV for LUMO, resulting in both levels being closer to one another; hence, the energy gap is lowered to 2.33 eV, reflecting a ∼39.98% decrease in E_g. A similar trend has been reported in previous theoretical studies, where the adsorption of TMZ on a $Be_{12}O_{12}$ nanocarrier reduced the energy gap from 9.93 eV to 6.85 eV. This agreement suggests that TMZ adsorption generally leads to a reduction in the HOMO–LUMO gap of nanocarrier systems due to electronic interactions between the drug molecule and the surface of the nanocarrier.[49] An increase in conductivity and reactivity of the nanosheet occurs with a reduction in the energy gap when the dominant peak arises. This change in the electronic structure means that the T-BN nanosheet will be more responsive and selective to TMZ and thus more useful for biosensor devices at the nanoscale. The dipole moment (D.M) for the most stable S_1 complex is 2.77 Debye. In water medium, the calculated HOMO–LUMO for the S_1 complex TMZ/T-BN is −5.87 eV (HOMO) and −3.59 eV

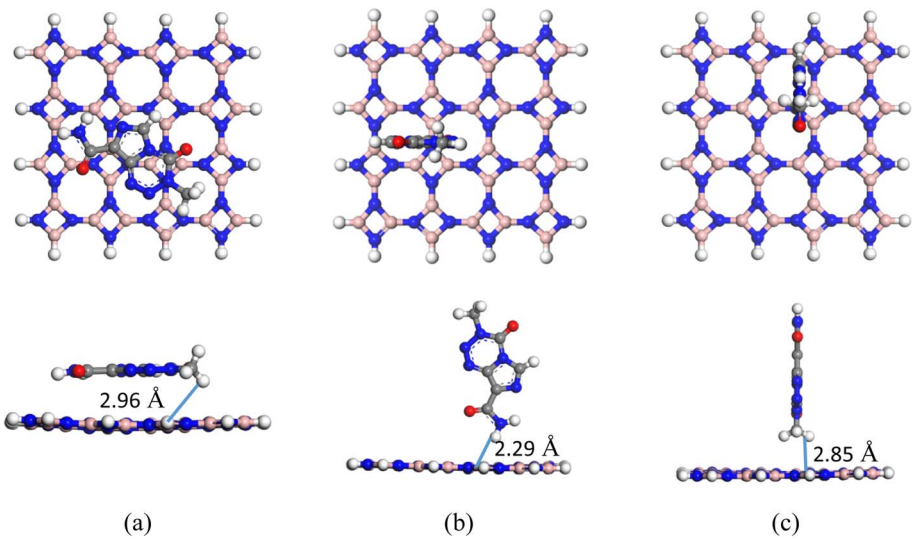

Fig. 3 Top and side views of the optimized structures for the (a) S_1, (b) S_2 and (c) S_3 configurations of the TMZ/T-BN complexes.

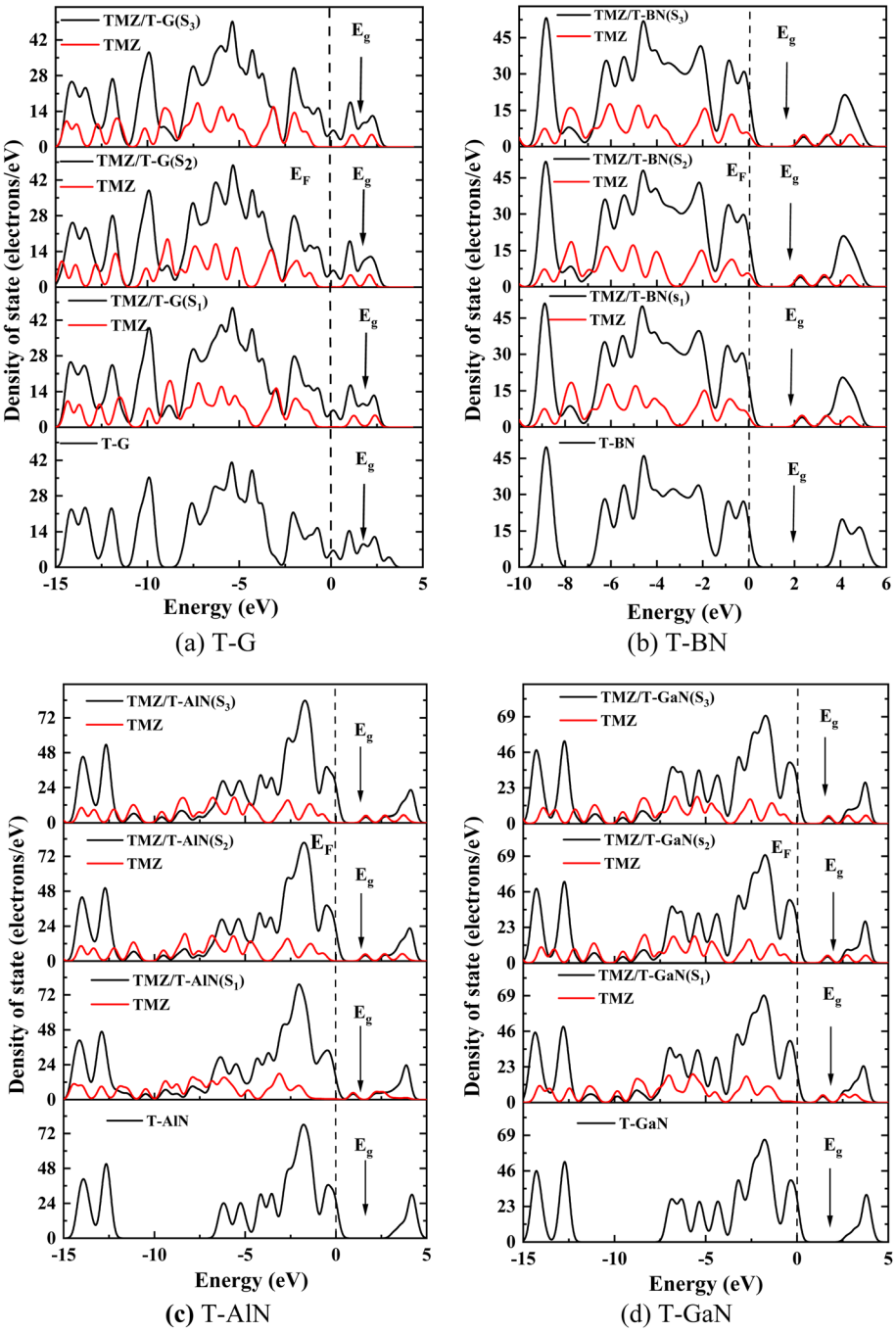

Fig. 4 Total and partial density of states (DOS) for (a) T-G, (b) T-BN, (c) T-AlN, and (d) T-GaN nanosheets before and after TMZ drug adsorption. The dashed lines represent the Fermi levels.

(LUMO). These values represent percentage changes in the energy gap of approximately 41.75%.

3.3 Adsorption of TMZ on T-AlN nanosheets

To enhance the adsorption capability of T-G towards the TMZ drug, Al and N atoms were introduced by substituting a central C atom in the T-G framework, forming the T-AlN structure. Three adsorption configurations of TMZ on T-AlN, S_1, S_2, and S_3, were investigated and are shown in Fig. 5. During the adsorption process, the T-AlN sheet exhibited a more pronounced distortion in the S_1 and S_3 configurations, while a downward deformation occurred in the S_2 configuration. The adsorption energies in the gas phase were calculated to be −1.56, −0.364, and −0.25 eV for the S_1, S_2, and S_3 configurations, respectively; the corresponding adsorption distances were 1.99 Å, 2.13 Å, and 2.89 Å. These values are summarized in Table 1. Mulliken charge-transfer analysis indicates that the TMZ drug molecule acts as an electron donor, with charge

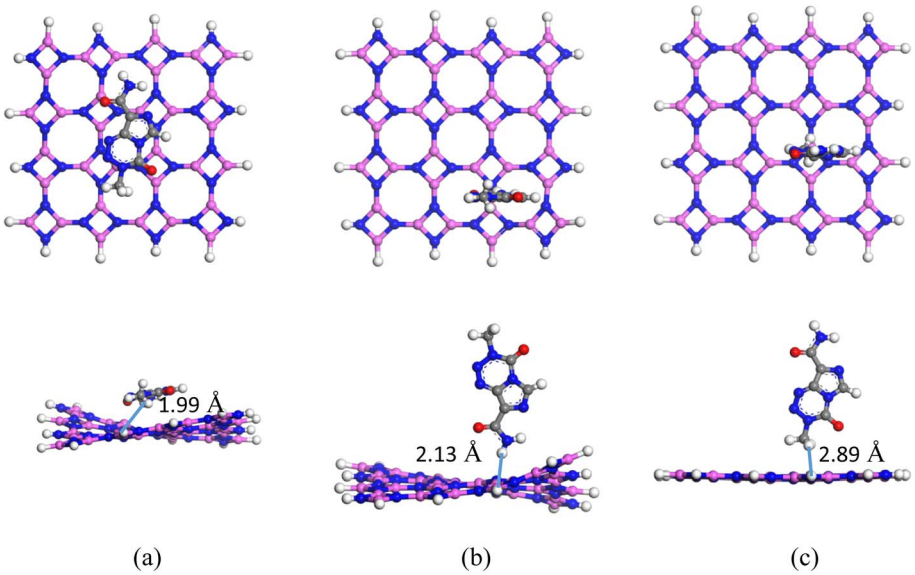

Fig. 5 Top and side views of the optimized structures for the (a) S_1, (b) S_2 and (c) S_3 configurations of the TMZ/T-AlN complexes.

transfers of $-0.015e$, $-0.04e$, and $-0.02e$ to the T-AlN sheet for S_1, S_2, and S_3, respectively. The relatively high adsorption energy, shorter interaction distance, and moderate to high charge transfer in the S_1 configuration suggest a strong interaction between TMZ and T-AlN, followed by moderate interaction in S_2 and weaker interaction in S_3. Electronic property analysis, including HOMO, LUMO, and E_g calculations, was performed and is detailed in Table 2. The HOMO levels of the S_1, S_2 and S_3 complexes were found to be -4.88, -5.05, and -5.15 eV, while the LUMO levels were -3.93, -3.43, and -3.49 eV, respectively. These results indicate a significant downward shift in LUMO energies and a slight shift in HOMO levels compared with those of pristine T-AlN ($E_{HOMO} = -5.1$ eV and $E_{LUMO} = -1.88$ eV), which originally had a band gap of 3.22 eV. Upon adsorption, the energy gap (E_g) reduced dramatically to 0.95 eV for S_1, 1.63 eV for S_2, and 1.66 eV for S_3. This corresponds to a percentage reduction in E_g of -70.48%, -49.47%, and -48.38% for S_1, S_2, and S_3, respectively. A similar trend has been reported in previous studies, where the adsorption of TMZ on Si- and Ge-decorated BN nanocages reduced the band gap by about 51.41% and 50.99%, respectively.[50] In the water medium, the calculated HOMO and LUMO energies for the S_1 complex of TMZ/T-AlN are -4.859 eV and -3.813 eV, respectively. These values represent percentage changes in the energy gaps of approximately -68.34%. Even the DOS plots of the TMZ/T-AlN complex reveal a noticeable reduction in the energy gap compared with pristine T-AlN. This band-gap narrowing originates from the hybridization between the electronic states of TMZ and the surface states of the T-AlN nanosheet upon adsorption. The emergence of new electronic

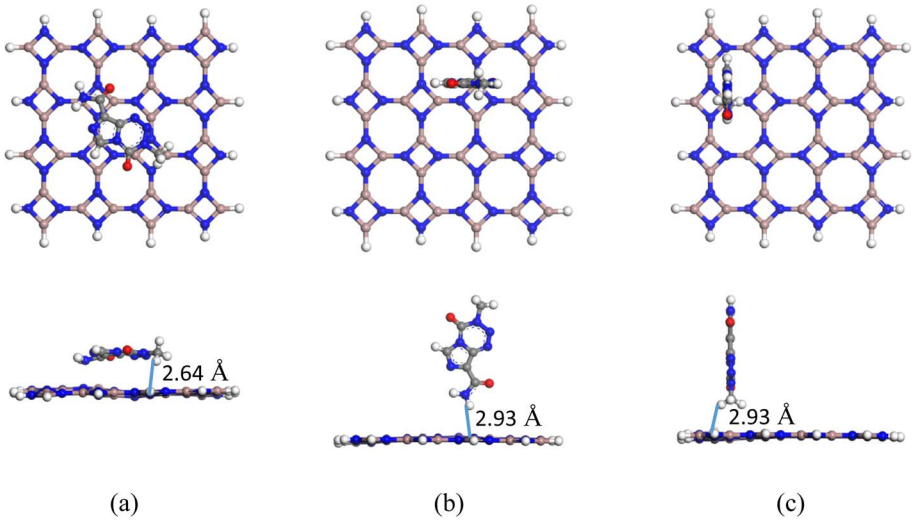

Fig. 6 Top and side views of the optimized structures for the (a) S_1, (b) S_2 and (c) S_3 configurations of the TMZ/T-GaN complexes.

states near the Fermi level indicates effective electronic coupling between the drug molecule and the carrier surface. The substantial reduction in E_g, especially in the S_1 complex, enhances electrical conductivity, thereby making the system more responsive for drug detection applications. These findings suggest that the introduction of Al and N dopants increases the reactivity and sensitivity of the T-G sheet; for the TMZ/T-AlN system in particular, the S_1 configuration shows promising potential for drug delivery applications.

3.4 Adsorption of TMZ on T-GaN nanosheets

We also investigated the impact of doping T-G with Ga and N atoms to form T-GaN nanosheets on the interaction with the TMZ drug molecule. Fig. 6 shows the optimized geometries for three different adsorption configurations of the TMZ/T-GaN complexes: S_1, S_2, and S_3. All three configurations exhibited negative adsorption energies, indicating favorable interactions between TMZ and the T-GaN nanosheet. Specifically, the adsorption energies in the gas phase were found to be −1.16, −0.18, and −0.25 eV for S_1, S_2, and S_3, respectively. The corresponding adsorption distances were 2.637 Å for S_1 and 2.928 Å for both S_2 and S_3. In terms of charge transfer, 0.042e was transferred from the nanosheet to TMZ in the S_1 configuration, suggesting a significant interaction. In contrast, minimal charge transfer was observed in S_2 (−0.017e) and S_3 (−0.014e). These results suggest that S_1 is the most stable configuration, where the TMZ molecule lies parallel to the surface, forming stronger interactions with the doped Ga atom. Notably, structural deformation of the T-GaN sheet was observed at the dopant site during adsorption in S_1 and S_3, indicating stronger interactions, while the deformation in S_2 was weaker. To assess the sensing capability of T-GaN towards TMZ, electronic characteristics, including HOMO, LUMO, and E_g, were analyzed (Fig. 7). The HOMO level of T-GaN was −5.037 eV, and the LUMO was −2.271 eV, resulting in a band gap of 2.766 eV. After adsorption in air medium, the HOMO–LUMO gaps for S_1, S_2, and S_3 decreased to 1.419 eV, 1.673 eV, and 1.736 eV, respectively. These changes correspond to significant reductions in the energy gap of −48.70%, −39.52%, and −37.24% for S_1, S_2, and S_3, respectively. In the water medium, the calculated HOMO and LUMO values for the S_1 complex of TMZ/T-GaN were −5.28 eV and −3.75 eV, respectively. These values represent percentage changes in the energy gaps of approximately −47.38%. The sharp decrease in band gap, especially for S_1, suggests enhanced electrical conductivity and chemical reactivity of the complex, implying that T-GaN nanosheets are highly sensitive to TMZ, particularly in the S_1 and S_3 configurations. Additionally, the dipole moment (D.M.) increased to 2.76D (S_1), 2.41D (S_2), and 3.52D (S_3) upon adsorption, further supporting the strong interaction and polarization effects induced by TMZ adsorption. In conclusion, among the configurations studied, S_1 exhibits the strongest interaction and highest sensitivity, making T-GaN a promising candidate for TMZ drug detection and delivery applications.

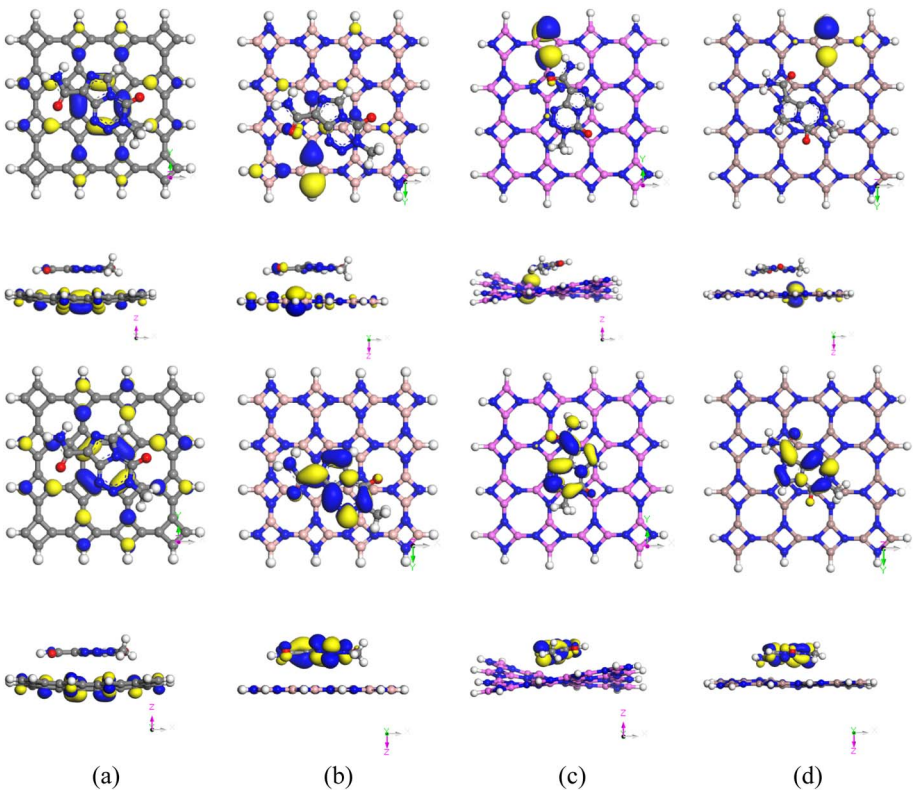

Fig. 7 Top and side views of the HOMO maps (top 2 rows) and LUMO maps (bottom 2 rows) of the S_1 configuration of the (a) TMZ/T-G, (b) TMZ/T-BN, (c) TMZ/T-AlN and (d) TMZ/T-GaN complexes.

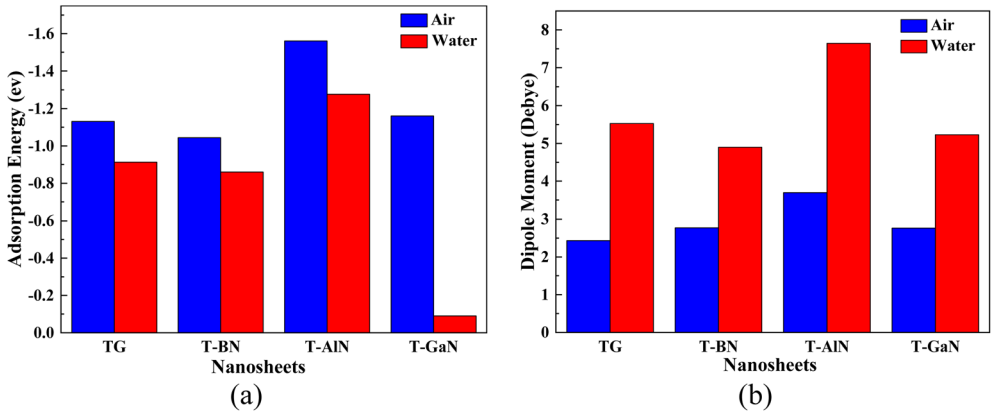

Fig. 8 Comparison of (a) adsorption energy and (b) dipole moments of the complexes in air and water environments.

3.5 Dipole moment

Dipole moment (D.M.) is a crucial concept in evaluating the charge transfer and reactivity between drug molecules and nanosheets. A high dipole moment indicates excellent charge redistribution and a strong interaction potential between the drug and the adsorbent surfaces.[51,52] In their pristine forms, the dipole moments of T-G, T-BN, T-AlN, and T-GaN nanosheets are all zero. However, the introduction of TMZ significantly alters the electronic distribution across these materials. Upon adsorption of the TMZ drug, the dipole moments increase notably across all the examined systems (Fig. 8). For the TMZ/T-G complexes, the dipole moments are 2.43*D* (S_1), 1.71*D* (S_2), and 3.63*D* (S_3). In the case of TMZ/T-BN, the corresponding values are 2.77*D*, 2.62*D*, and 3.33*D*, respectively. For TMZ/T-AlN, dipole moments increase to 3.7*D*, 2.47*D*, and 3.3*D* for the S_1, S_2, and S_3 complexes, respectively. Finally, the TMZ/T-GaN system exhibits dipole moments of 2.76*D*, 2.41*D*, and 3.52*D*, respectively. This considerable rise in dipole moment following TMZ adsorption reflects significant charge transfer and indicates a complex and strong interaction between the drug molecule and the nanosheet surfaces, as shown in Table 2. A comparable trend has been reported in previous studies; for example, the dipole moment of isolated temozolomide (3.34*D*) increased significantly to 6.90*D* after adsorption on HCM-cellulose, indicating enhanced polarity of the adsorption complex. This agreement suggests that TMZ adsorption on nanocarrier surfaces generally leads to increased dipole moments due to charge transfer and polarization effects within the system.[53]

3.6 Drug release

The drug-release mechanism is a crucial element for evaluating the efficiency of a drug-delivery system. In this study, the desorption times of TMZ from various nanosheets were calculated using the van't Hoff–Arrhenius equation derived from transition-state theory:

$$\tau = \frac{1}{\nu_0}\exp\left(\frac{-E_{ad}}{k_B T}\right), \quad (11)$$

where T represents the temperature (in Kelvin), with calculations performed at room temperature (298 K), normal body temperature (310 K), and cancer tissue temperature (315 K). The attempt frequency (ν_0) is assumed to be 10^{18} Hz, and k_B is the Boltzmann constant. The desorption time (τ) depends exponentially on the adsorption energy (E_{ads}). Among the nanosheets studied, T-

Table 3 Calculated release times of the TMZ drug in gas and water phases at 298 K (room temperature), 310 K (body temperature), and 315 K (cancer tissue temperature)

	Air medium			Water medium		
Nanosheets	298 K	310 K	315 K	298 K	310 K	315 K
T-G	1.35×10^{1}	2.44×10^{0}	1.25×10^{0}	2.71×10^{-3}	6.84×10^{-4}	3.97×10^{-4}
	6.52×10^{-15}	4.64×10^{-3}	4.06×10^{-3}	—	—	—
	1.09×10^{-13}	6.94×10^{-14}	5.81×10^{-14}	—	—	—
T-BN	4.58×10^{-1}	9.48×10^{-2}	5.1×10^{-2}	3.53×10^{-4}	9.67×10^{-5}	5.79×10^{-5}
	2.16×10^{-14}	1.47×10^{-14}	1.26×10^{-14}	—	—	—
	2.45×10^{-14}	1.66×10^{-14}	1.42×10^{-14}	—	—	—
T-AlN	2.52×10^{8}	2.39×10^{7}	9.48×10^{6}	3.93×10^{3}	5.73×10^{-2}	2.68×10^{2}
	1.45×10^{-12}	8.37×10^{-13}	6.74×10^{-13}	—	—	—
	1.48×10^{-14}	1.02×10^{-14}	8.84×10^{-15}	—	—	—
T-GaN	4.29×10^{1}	7.47×10^{0}	3.75×10^{0}	1.81×10^{-3}	4.65×10^{-4}	2.72×10^{-4}
	9.68×10^{-16}	7.42×10^{-16}	6.68×10^{-16}	—	—	—
	1.82×10^{-14}	1.24×10^{-14}	1.1×10^{-14}	—	—	—

Table 4 Chemical potential (μ), global hardness (η) and electrophilicity index (ω) (eV), global softness (S) (eV^{-1}), and nucleophilicity index (ν) (eV^{-1}) of the complexes in the gas phase

Complex	State	μ (eV)	η (eV)	S (eV^{-1})	ω (eV)	ν (eV^{-1})
T-G		4.08	0.12	4.15	68.95	0.015
TMZ/T-G	S_1	4.11	0.122	4.10	69.26	0.014
	S_2	4.09	0.124	4.02	67.07	0.015
	S_3	4.18	0.121	4.12	71.99	0.014
T-BN		3.66	1.939	0.26	3.46	0.29
TMZ/T-BN	S_1	4.42	1.164	0.43	8.395	0.12
	S_2	4.44	1.129	0.44	8.74	0.11
	S_3	4.5	1.196	0.42	8.46	0.12
T-AlN		3.49	1.609	0.31	3.78	0.26
TMZ/T-AlN	S_1	4.40	0.475	1.05	20.45	0.05
	S_2	4.24	0.813	0.61	11.07	0.09
	S_3	4.32	0.831	0.60	11.24	0.09
T-GaN		3.65	1.383	0.36	4.83	0.21
TMZ/T-GaN	S_1	4.23	0.71	0.70	12.62	0.08
	S_2	4.19	0.84	0.60	10.49	0.095
	S_3	4.22	0.87	0.58	10.24	0.098

AlN(P) exhibited the highest adsorption energy in both air (−1.561 eV) and water media (−1.277 eV). Drug release times of 9.45×10^6 s and 2.68×10^2 s were recorded in air and water media, respectively, at 315 K (Table 3).

This indicates a strong binding of TMZ to the T-AlN nanosheet, potentially suggesting slow drug release. Other promising interactions were observed for T-GaN (S_1) and T-G (S_1), with desorption times in air media of 3.74 s and 1.247 s, respectively, at 315 K, and in water media of 2.73×10^{-4} s and 3.97×10^{-4} s, respectively, at the same temperature (Table 3). In contrast, S_2 and S_3 variants of the nanosheets showed much weaker adsorption energies (from −0.176 to −0.364 eV) and extremely short desorption times (typically in the range of 10^{-15} to 10^{-12} s), suggesting rapid release of TMZ and potentially lower loading efficiency. A similar relationship between adsorption strength and recovery time has been reported for TMZ adsorption on $Be_{12}O_{12}$ and $B_{12}N_{12}$ nanocage carriers, where stronger adsorption interactions resulted in longer drug recovery times, highlighting the crucial role of adsorption energy in controlling the release behavior of TMZ from nanostructured carriers.[49] These findings imply that T-AlN(S_1), T-GaN(S_1), and T-G (S_1) nanosheets are the most promising candidates for sustained TMZ release under physiological and pathological conditions.

3.7 Quantum molecular descriptors

The structural reactivity of the complexes was assessed in both air and water media using quantum molecular descriptors (QMDs), including chemical potential (μ), global hardness (η), global softness (S), and the electrophilicity index (ω) (Tables 4 and 5). Here, μ indicates the tendency of a molecule to release electrons; a larger absolute value generally corresponds to higher chemical reactivity. After drug adsorption, μ increased for all S_1 configurations of the studied complexes, indicating enhanced chemical reactivity. For instance, in the air medium, the value of μ increased from 4.076 to 4.11, 3.66 to 4.42, 3.49 to 4.41, and 3.65 to 4.23 eV. Similarly, in water medium, μ increased from 4.46 to 4.47, 3.91 to 4.73, 3.49 to 4.34, and 3.9 eV to 4.52 eV. Also, η decreased in most cases after adsorption, which implies improved charge-transfer properties and enhanced reactivity. For example, η decreased from 1.94 to 1.164 in T-BN, 1.61 to 0.47 in T-AlN, and 1.38 to 0.71 in T-GaN in air medium and from 1.95 to 1.14 in T-BN, 1.65 to 0.52 in T-AlN, and 1.45 to 0.76 in T-GaN in water medium. In contrast, the change in T-G was minor, which indicated a relatively consistent hardness profile. As expected, softness defined as the inverse of hardness, increased significantly for the majority of the systems after drug adsorption. The value of S increased from 0.26 to 0.43, 0.31 to 1.0 and 0.36 to 0.71 in the air medium and from 0.26 to 0.43, 0.30 to 0.96, and 0.34 to 0.65 in the water medium, further validating the improved chemical reactivity and charge accommodation of the system post-adsorption. A slight decrease was observed in T-G from 4.15 to 4.10, 3.95 to 3.79 in air and water medium, reflecting minor rigidity. The electrophilicity index (ω), a measure of the molecule's ability to accept electrons, also exhibited notable changes.[54] In T-G, ω increased slightly from 68.95 to 69.26 eV (S_1) but varied more significantly across other materials in air medium. T-BN showed an increase from 3.46 to 8.40 eV, T-AlN from 3.78 to 20.45 eV, and T-GaN from 4.83 to 12.62 eV in the respective S_1 configurations, indicating stronger electron-accepting capabilities post-adsorption. Overall, the variations in QMDs after drug adsorption in air medium confirm that the interaction modifies the electronic properties of the nanosheets. In water medium, these electronic structure variations confirm that TMZ

Table 5 Chemical potential (μ), global hardness (η), and electrophilicity index (ω) (eV), global softness (S) (eV^{-1}), nucleophilicity index (ν) (eV^{-1}), HOMO energies (E_{HOMO}), LUMO energies (E_{LUMO}), and energy gap (E_g) (eV), and energy gap variation (% ΔE_g) of the complexes in the water phase

Complex	E_{HUMO} (eV)	E_{LUMO} (eV)	μ (eV)	η (eV)	S (eV^{-1})	ω (eV)	ν (eV^{-1})	E_g (eV)	% ΔE_g
T-G	−4.59	−4.34	4.47	0.13	3.95	78.82	0.01	0.25	
TMZ/T-G	−4.58	−4.33	4.46	0.132	3.79	75.24	0.013	0.26	4.35
T-BN	−5.86	−1.96	3.91	1.95	0.26	3.92	0.26	3.9	
TMZ/T-BN	−5.87	−3.59	4.73	1.14	0.44	9.83	0.1	2.27	−41.75
T-AlN	−5.16	−1.85	3.5	1.65	0.30	3.72	0.27	3.3	
TMZ/T-AlN	−4.86	−3.81	4.34	0.52	0.96	17.97	0.06	1.05	−68.34
T-GaN	−5.35	−2.45	3.9	1.45	0.34	5.24	0.19	2.9	
TMZ/T-GaN	−5.28	−3.75	4.52	0.76	0.65	13.35	0.08	1.53	−47.38

adsorption leads to significant modification in the frontier molecular orbitals and chemical reactivity of the tetragonal nanosheets in the water phase. Among them, T-AlN and T-GaN show the most substantial changes in terms of softness and electrophilicity, implying stronger interaction and better potential as drug-delivery carriers.

3.8 Work function

The work function (φ) represents the minimum energy required to remove an electron from the Fermi level to an infinite distance and plays a crucial role in evaluating the effect of drug adsorption on nanosheets. It is calculated using the following equation:

$$\Phi = V_{el}(+\infty) - E_F, \quad (12)$$

where $V_{el}(+\infty)$ is the electrostatic potential far from the surface, which is approximated to zero; hence, the work function becomes numerically equal to the negative Fermi level energy level:

$$\Phi = -E_F. \quad (13)$$

To assess the impact of drug adsorption, the percentage change in the work function was calculated as follows:

$$\%\ \phi = \left(\frac{\phi_A - \phi_B}{\phi_B}\right) \times 100, \quad (14)$$

where Φ_B and Φ_A denote the work functions before and after adsorption, respectively. A change in φ alters the gate voltage, induces an electrical signal, and is a useful indicator for chemical sensing applications.[55] The calculated Fermi levels and corresponding work functions before and after the adsorption of the TMZ drug on the T-G, T-BN, T-AlN, and T-GaN nanosheets are listed in Table 3. The intrinsic work function values of T-G, T-BN, T-AlN, and T-GaN were found to be 4.075, 3.647, 3.391, and 3.554 eV, respectively. After TMZ adsorption, noticeable changes in the work function were observed. For the T-G nanosheet, φ increased slightly in all configurations, with the highest change being 2.58% in S_3. T-BN showed substantial increases, with a maximum change of 21.06% in S_3. The T-AlN nanosheet exhibited the most significant work function variation, reaching up to 28.36% in S_1. For T-GaN, the change was also notable, with values ranging from 15.14% to 16.96%. These results highlight that the T-AlN nanosheet experiences the greatest variation in work function upon TMZ adsorption, indicating strong interaction and high sensitivity, making it a promising candidate for TMZ drug sensing. T-BN and T-GaN also show considerable changes, suggesting their potential utility as sensor materials. In contrast, the lower variation in T-G indicates weaker sensitivity toward TMZ.

3.9 COSMO surface analysis

When drug-carrier complexes are administered into the tissue cell, water molecules surround them. Therefore, understanding the behavior of these systems in aqueous environments is crucial for evaluating drug delivery efficacy. We investigated the influence of the solvent on the adsorption behavior of TMZ on tetragonal nanosheets, as well as the corresponding changes in their electronic properties. In addition, COSMO surface analysis was performed to assess the polarity and charge distribution of the complexes in the presence of a polar solvent. Fig. 9 displays the COSMO surfaces of the nanosheets and their corresponding TMZ-loaded complexes: (a) T-G, (b) T-BN, (c) T-AlN, and (d) T-GaN. The red regions indicate hydrogen-bond donor (HBD) zones, areas of significant positive charge, while the blue regions represent hydrogen-bond acceptors (HBA) zones, areas of strong negative polarity.[56,57] Neutral or non-polar areas are shown in green. Before adsorption, the nanosheets largely exhibit uniform polarity, as seen in the upper row of Fig. 9. However, after TMZ adsorption (bottom row), distinct polar zones appear due to molecular interactions between the drug and the nanosheets. In the T-G/TMZ complex shown in Fig. 9(a),

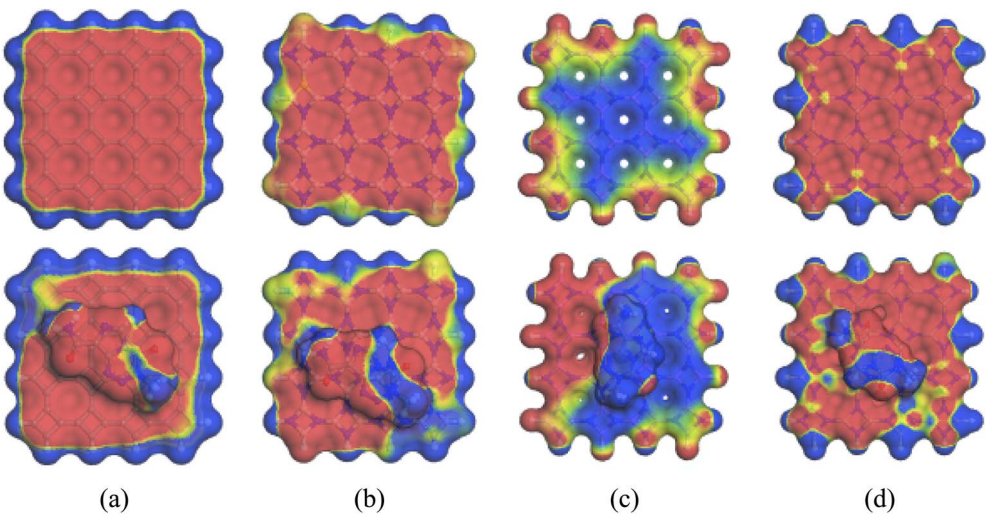

Fig. 9 COSMO surfaces of TMZ on (a) T-G, (b) T-BN, (c) T-AlN, and (d) T-GaN before and after adsorption.

intense HBD regions emerge on the nanosheet, particularly away from the edges, while HBA zones concentrate around the TMZ molecule. For the T-BN system shown in Fig. 9(b), HBD characteristics localize along the B–N bonds of the nanosheet, and the drug again contributes predominantly to the HBA regions. A similar trend is observed in the T-AlN and T-GaN based systems shown in Fig. 9(c) and (d), where strong polarization appears around the sulfur-containing groups of TMZ, which act as HBD sites, whereas the opposite side of the complex shows dominant HBA features. These polar interactions confirm the role of TMZ's electron-rich regions in enhancing intermolecular binding. This COSMO surface analysis aligns well with the previously observed increases in dipole moments after drug adsorption, confirming that the adsorption of TMZ enhances the overall polarity of the nanosheet–drug complexes in water. Such polarity changes may significantly impact the solubility, stability, and biological interaction of the complexes, thus contributing to their effectiveness as drug delivery platforms.

4 Conclusions

In this study, DFT calculations were employed to systematically investigate the adsorption characteristics and electronic responses of tetragonal nanosheets T-G, T-BN, T-AlN, and T-GaN toward the anticancer drug TMZ in both gas and aqueous media. Among the three explored adsorption configurations (S_1, S_2, and S_3), the S_1 state consistently exhibited the most favorable interaction across all nanosheets. The adsorption energies indicated that TMZ interacts strongly with T-AlN (−1.56 eV) and T-GaN (−1.16 eV) in the gas phase, while significant adsorption was also retained in aqueous conditions. Mulliken charge analysis revealed notable charge transfer from TMZ to T-AlN and T-GaN, reinforcing their potential for drug sensing and delivery. A marked reduction in HOMO–LUMO energy gaps up to −70.48% for T-AlN and −48.70% for T-GaN was observed, highlighting enhanced conductivity and chemical reactivity post-adsorption. Dipole moment and COSMO surface analyses confirmed enhanced polarity and solubility in water upon TMZ loading, especially for the T-AlN and T-GaN systems. The work function of these nanosheets also shifted significantly after adsorption, indicating strong interaction potential and sensitivity to electronic perturbations. Taken together, these findings suggest that, among the studied nanomaterials, T-AlN and T-GaN nanosheets exhibit the most promising features as nanocarriers for TMZ, owing to their strong adsorption, enhanced electronic reactivity, favorable desorption dynamics, and high polarity in aqueous environments. These insights pave the way for their application in targeted and efficient drug-delivery systems for cancer therapy.

Conflicts of interest

The authors have declared no conflict of interest.

Data availability

All data supporting the findings of this study, including the optimized structures, adsorption energy values, charge transfer, and work function, are available within the article. All the calculations have been implemented by the DMol^3 module in BIOVIA Materials Studio 2017. Additional data can be provided by the corresponding author upon reasonable request.

Acknowledgements

We thankfully acknowledge the Bangladesh Research and Education Network (BdREN) for the computational access. Artificial intelligence (AI) tools were used solely for improving the grammar, language, and clarity of the manuscript. The authors ensured that the scientific content, interpretations, and conclusions were entirely their own and were not influenced by the AI tools used.

References

1 I. Munir, M. Perveen, S. Nazir, R. A. Khera, A. R. Ayub, K. Ayub and J. Iqbal, *J. Mol. Liq.*, 2021, **336**, 116327.
2 L. Jiang, L. Li, X. He, Q. Yi, B. He, J. Cao, W. Pan and Z. Gu, *Biomaterials*, 2015, **52**, 126–139.
3 G. Tan, Y. Zhong, L. Yang, Y. Jiang, J. Liu and F. Ren, *Chem. Eng. J.*, 2020, **390**, 124446.
4 C. Holohan, S. Van Schaeybroeck, D. B. Longley and P. G. Johnston, *Nat. Rev. Cancer*, 2013, **13**(10), 714–726.
5 S. Pasban and H. Raissi, *Sci. Rep.*, 2021, **11**(1), 1–9.
6 N. Masnabadi, S. Masoudi and M. Hosseinzadeh, *Lett. Org. Chem.*, 2024, **21**, 655–668.
7 A. R. Ayub, G. Basharat, S. Arshad, S. Nazir, H. Hamid, S. M. Arshed, M. N. Zahid, J. Iqbal and K. Ayub, *J. Mol. Graph. Model.*, 2023, **125**, 108611.
8 Y. Cao, S. Alamri, A. A. Rajhi, A. E. Anqi and M. Derakhshandeh, *Mater. Chem. Phys.*, 2022, **275**, 125260.
9 A. Sultana, M. Zare, V. Thomas, T. S. S. Kumar and S. Ramakrishna, *Mod. Drug Discov.*, 2022, **15**, 100134.
10 A. Gholami, E. Shakerzadeh, E. Chigo Anota and M. corazon Flores Bautista, *Inorg. Chem. Commun.*, 2023, **148**, 110326.
11 M. Jezierzański, N. Nafalska, M. Stopyra, T. Furgoł, M. Miciak, J. Kabut and I. Gisterek-Grocholska, *Curr. Oncol.*, 2024, **31**, 3994–4002.
12 A. Mortazavifar, H. Raissi and A. Akbari, *J. Mol. Liq.*, 2019, **276**, 577–587.
13 G. A. Okon, D. G. Malu, H. Y. Abdullah, C. R. Nwokoye, N. I. Gber, C. P. Egbo, J. A. Unyime and T. E. Gber, *Diam. Relat. Mater.*, 2024, **149**, 111628.
14 M. D. Mohammadi, H. Y. Abdullah, H. Louis, E. E. Etim, H. O. Edet and O. C. Godfrey, *Chem. Phys. Impact*, 2023, **6**, 100234.
15 K. W. Qadir, M. D. Mohammadi, F. K. M. Alosfur and H. Y. Abdullah, *J. Mol. Model.*, 2025, **31**, 20.
16 T. J. Lu, B. Lienhard, K. Y. Jeong, H. Moon, A. Iranmanesh, G. Grosso and D. Englund, *ACS Photonics*, 2020, **7**, 2650–2657.

17 Y. Cao, M. Farahmand, S. Fosshat, S. Rezaei, L. Pourmomen Arabi and P. Liu, *Comput. Theor. Chem.*, 2022, **1207**, 113537.
18 E. A. Eno, H. Louis, P. S. Akpainyang, O. J. Ikenyirimba, T. O. Unimuke, O. E. Offiong and A. S. Adeyinka, *ACS Appl. Energy Mater.*, 2023, **6**, 4437–4452.
19 M. M. Kadhim, Z. T. Abed, R. Rayid, S. A. Abdullaha, A. Majdi, A. M. Rheima and S. K. Hachim, *Comput. Theor. Chem.*, 2023, **1220**, 113982.
20 K. W. Qadir, M. D. Mohammadi and H. Y. Abdullah, *Comput. Theor. Chem.*, 2025, **1244**, 115063.
21 K. W. Qadir, M. D. Mohammadi, F. K. M. Alosfur and H. Y. Abdullah, *J. Mol. Model.*, 2025, **31**, 20.
22 M. Doust Mohammadi, H. Y. Abdullah, H. Louis, E. E. Etim and H. O. Edet, *J. Mol. Liq.*, 2023, **387**, 122621.
23 J. Siqi, Y. Shasha, W. Xiao and W. Gu, *Mol. Phys.*, 2020, **118**(18), e1757775.
24 G. Jouonang Létché, A. D. Tamafo Fouegue, V. de P. Zoua, R. Abdoul Ntieche and G. B. Noumi, *Mater. Sci. Semicond. Process.*, 2025, **185**, 108980.
25 B. L. N. Wandji, A. D. T. Fouegue, N. K. Nkungli, R. A. Ntieche and A. Wahabou, *R. Soc. Open Sci.*, 2022, **9**(4), 211650.
26 M. A. A. Ibrahim, A. S. S. M. Rady, P. A. Sidhom, S. R. M. Sayed, K. E. Ibrahim, A. M. Awad, T. Shoeib and L. A. Mohamed, *ACS Omega*, 2024, **9**, 25203–25214.
27 M. A. A. Ibrahim, M. H. A. Hamad, A. H. M. Mahmoud, G. A. H. Mekhemer, P. A. Sidhom, S. R. M. Sayed, N. A. M. Moussa, A. I. M. Rabee, E. Dabbish and T. Shoeib, *RSC Adv.*, 2023, **13**, 17465–17475.
28 M. N. Sakib, T. Ahmed, M. A. Shafiulla, D. F. Afroj, A. A. Piya and S. U. D. Shamim, *AIP Adv.*, 2024, **14**(3), 035230.
29 G. G. R. Ortiz, B. Cespedes-Panduro, S. A. Shahrtash, F. Rahimi, S. Sandi, J. L. Arias-Gonzáles, A. A. Ramírez-Coronel, J. C. Cotrina-Aliaga, M. H. Lafta, B. Abedi Kiasari and R. Akhavan-Sigari, *Diam. Relat. Mater.*, 2023, **135**, 109800.
30 A. D. Tamafo Fouegue, V. de Paul Zoua, G. N. Kounou, B. L. Ndjopme Wandji, J. N. Ghogomu and R. A. Ntieche, *Nanoscale Adv.*, 2023, **5**, 5880–5891.
31 H. Di Ma, J. Y. Liu, W. H. Chen, Z. Wei, Y. Li, Y. F. Liu and C. C. Du, *J. Mol. Liq.*, 2024, **406**, 125124.
32 B. Delley, *J. Chem. Phys.*, 2000, **113**, 7756–7764.
33 J. P. Perdew, K. Burke and M. Ernzerhof, *Phys. Rev. Lett.*, 1996, **77**, 3865.
34 S. Grimme, *J. Comput. Chem.*, 2006, **27**, 1787–1799.
35 B. Delley, *Phys. Rev. B: Condens. Matter Mater. Phys.*, 2002, **66**, 155125.
36 M. J. Ungerer, C. G. C. E. van Sittert, D. J. van der Westhuizen and H. M. Krieg, *Comput. Theor. Chem.*, 2016, **1090**, 112–119.
37 B. Delley, *Mol. Simul.*, 2006, **32**, 117–123.
38 C. Xiao, K. Ma, G. Cai, X. Zhang and E. Vessally, *J. Mol. Graph. Model.*, 2020, **96**, 107539.
39 R. G. Pearson, *J. Org. Chem.*, 1989, **54**, 1423–1430.
40 P. Fuentealba and C. Cárdenas, *Chem. Modell.*, 2015, **11**, 151–174.
41 A. Piya, T. Ahmed, M. Khaleque, K. Ahmed and S. U. D. Shamim, *Comput. Theor. Chem.*, 2022, **1217**, 113902.
42 S. Shahab, R. Kumar, M. Sheikhi, Z. Ihnatovich, J. Siniutsich, E. Koroleva, L. Filippovich, A. Auhustsinovich, M. Makhakhei, M. Stati, W. Hui, M. Khancheuski and M. Y. Borzehandani, *Anal. Chem. Lett.*, 2024, **14**, 638–653.
43 R. A. Yossa Kamsi, G. W. Ejuh, Y. Tadjouteu Assatse, C. A. Njeumen, F. Tchoffo and J. M. B. Ndjaka, *Chin. J. Phys.*, 2019, **60**, 1–11.
44 A. Goyal, D. Aggarwal, S. Kapoor, N. Goel, S. Singhal and J. Shukla, *New J. Chem.*, 2020, **44**, 3985–3997.
45 J. Princy Maria, V. Nagarajan and R. Chandiramouli, *Chem. Phys. Lett.*, 2020, **738**, 136841.
46 K. Fukui, *Science*, 1982, **218**, 747–754.
47 M. Roy Swarna, M. Hasan Opi, T. Ahmed, A. A. Piya, U. Habiba and S. U. D. Shamim, *Nanoscale Adv.*, 2024, **6**(23), 5988–6007.
48 S. Jameh-Bozorghi and H. Soleymanabadi, *Phys. Lett. A*, 2017, **381**, 646–651.
49 M. A. A. Ibrahim, A. S. S. M. Rady, P. A. Sidhom, S. R. M. Sayed, K. E. Ibrahim, A. M. Awad, T. Shoeib and L. A. Mohamed, *ACS Omega*, 2024, **9**, 25203–25214.
50 L. Wei, J. Lei, T. Luo and L. Wu, *Struct. Chem.*, 2020, **31**, 2321–2331.
51 Z. Khodadadi and L. Torkian, *Mater. Res. Express*, 2019, **6**, 065058.
52 R. Chandiramouli, A. Srivastava and V. Nagarajan, *Appl. Surf. Sci.*, 2015, **351**, 662–672.
53 M. Shahi and F. Azarakhshi, *BMC Chem.*, 2023, **17**, 114.
54 P. K. Chattaraj, U. Sarkar and D. R. Roy, *Chem. Rev.*, 2006, **106**, 2065–2091.
55 N. Sharma, R. Kakkar, P. Bansal, A. Singh, H. Ojha, D. P. Pathak and R. K. Sharma, *Inorg. Chim. Acta*, 2019, **484**, 111–124.
56 T. Aissaoui, Y. Benguerba and I. M. AlNashef, *J. Mol. Struct.*, 2017, **1141**, 451–456.
57 K. J. Suthar and M. H. Joshipura, *Chem. Eng. J. Adv.*, 2021, **7**, 100132.